Predictions in Ungauged Basins: Promise and Progress (Proceedings of symposium S7 held during the Seventh IAHS Scientific Assembly at Foz do Iguaçu, Brazil, April 2005). IAHS Publ. 303, 2006.

Influence of spatial variability of precipitation in a distributed rainfall–runoff model

TAPASH DAS[1], ANDRÁS BÁRDOSSY[1] & ERWIN ZEHE[2]

1 *Institute of Hydraulic Engineering, University of Stuttgart, Pfaffenwaldring 61, D-70569 Stuttgart, Germany*
tapash@iws.uni-stuttgart.de

2 *Institute for Geoecology, University of Potsdam, Germany*

Abstract The objective of this research was to examine the influence of the spatial variability of precipitation data from different sources on the accuracy of runoff simulation. In this study, interpolated precipitation by external drift kriging and conditional simulated precipitation based on turning band simulation are used to represent the spatial variability of precipitation. Also, the precipitation is averaged over different spatial scales ranging from 4 km^2 to 614 km^2. The original and averaged precipitation is used as a main forcing input in a conceptual distributed rainfall–runoff model. An automatic calibration method based on the combinatorial optimization algorithm simulated annealing is applied. Also, the aggregated Nash-Sutcliffe coefficients at different time scales are used as objective function in the study. The simulated hydrographs obtained using original and averaged precipitation are analysed through comparisons of the Nash-Sutcliffe coefficient and other goodness-of-fit indexes. By means of them, the influence of spatial variability of precipitation data on the accuracy of simulated runoff is assessed.

Key words conditional simulation; distributed modelling; simulated annealing; spatial variability

INTRODUCTION

Hydrological modelling and forecasting require precipitation data as one of the most important inputs. Precipitation often varies significantly over space and time within a basin. Thus in a rainfall–runoff model, the accurate knowledge of precipitation is needed for an accurate river discharge estimation. This is due to the fact that precipitation plays a vital role in determining surface hydrological processes (Haddeland *et al.*, 2002). For example, the effect of the spatial variability of precipitation on the response of small basins has been investigated by many researchers using either observed rainfall (Obled *et al.*, 1994; Lopes, 1996; Liang *et al.*, 2004) or stochastic precipitation models (Wilson *et al.*, 1979; Krajewski *et al.*, 1991). Rationally, point measurements of raingauge accumulations that are distributed in space over the river basin are converted to areal rainfall using interpolation techniques like kriging, Thiessen polygons, and the inverse distance method. In contrast, weather radar offers enormous potential for hydrological applications because it is an important source for rainfall amount distribution over space and time and covers large regions (Smith *et al.*, 1996; Finnerty *et al.*, 1997). Based on the previous research outcomes, raingauge precipitation is still an important source of data for improving the radar and its operational purposes.

The purpose of the present study is to investigate the impact of spatial variability of precipitation on the hydrological modelling results for a mesoscale catchment. Precipitation interpolated by external drift kriging and conditional simulated precipitation based on turning band simulation were used to represent the spatial variability of precipitation. The distributed HBV-IWS rainfall–runoff model was applied to carry out the study objectives. The Upper Neckar catchment was selected as a test catchment. The model performance was assessed through the analysis of the simulated hydrographs and the computation of goodness-of-fit indexes.

FRAMEWORK OF THE ANALYSIS

Study catchment description

The Upper Neckar catchment is located in western Germany. Figure 1 shows the study area together with the Neckar River and Plochingen gauging station. The area covered by the Upper Neckar catchment is about 4000 km^2, which is approximately 30% of the whole Neckar catchment. The maximum and minimum elevation of the catchment are 1000 m a.s.l. and 250 m a.s.l, respectively.

The continental and oceanic climate has an impact on the weather of the study area. This is due to the prevailing westerly winds within the region and the impact of the Atlantic Ocean, which is relatively strong. The second major impact on the climate is the topography.

In the Upper Neckar catchment the mean annual precipitation is 950 mm and ranges from 700 mm to 1680 mm. The mean daily temperature in the catchment is 8.8°C.

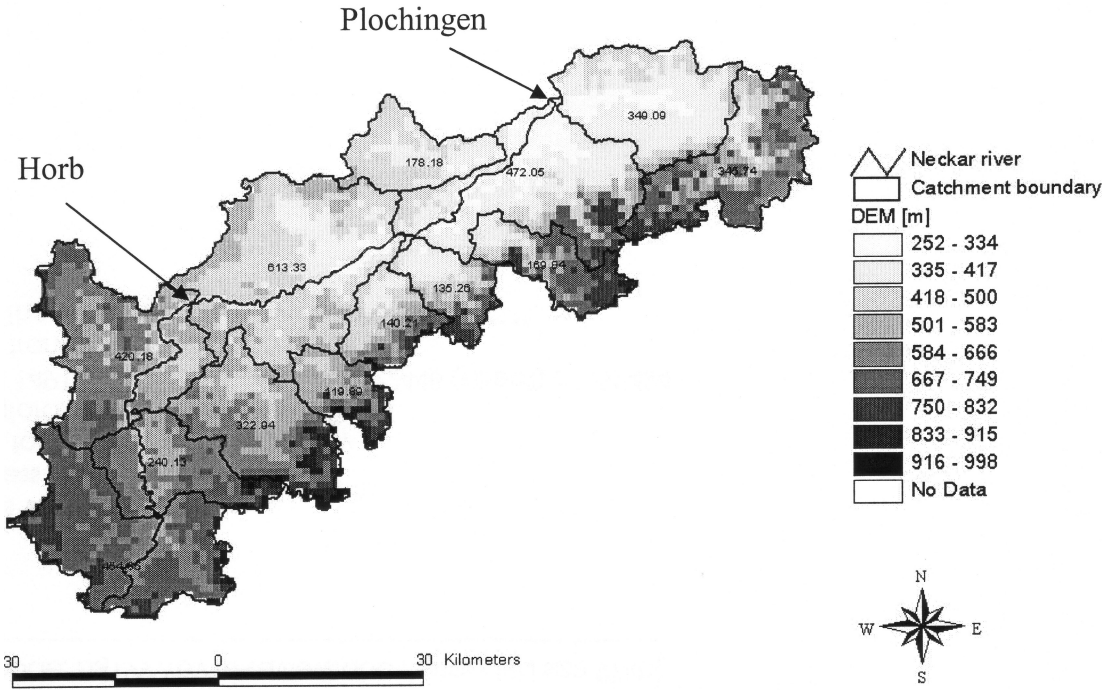

Fig. 1 The catchment study area and the Neckar River (the number within each sub-catchment indicates the area in km^2).

The natural vegetation in the Upper Neckar catchment has been influenced by human activities; part of the natural vegetation was replaced by forest (commercial) and arable land. Coniferous trees are the most dominating vegetation, especially in the western part, close to the Black Forest. The mean runoff at the outlet gauging station Plochingen is 46.93 $m^3 s^{-1}$.

Brief description of the model

The modified HBV-IWS rainfall–runoff model was applied in this study. The HBV-IWS model was developed in the Institute of Hydraulic Engineering, University of Stuttgart, Germany, based on the HBV model (Bergström & Forsman, 1973) concept. Originally, the HBV model was developed at the Swedish Hydrological and Meteorological Institute (SMHI) for runoff simulation and hydrological forecasting, but the fields of application have increased steadily over the last decades.

The HBV-IWS rainfall–runoff model is a semi-distributed conceptual model. The area to be modelled is divided into a number of sub-catchments and each sub-catchment is further divided into a number of zones. The dynamic of the different flow components at the sub-catchment scale is conceptually represented by two reservoirs. The Upper reservoir simulates the rapid and delayed interflow in the sub surface layer, while the lower reservoir represents the base flow. Both reservoirs are connected in series by a constant percolation rate and are considered linear with a recession coefficient. Finally there is a transformation function for smoothing the generated flow. The transformation consists of a triangular weighting function with one free parameter. In the existing HBV-IWS model structure, the sub-catchment is divided into a number of zones according to elevation, land use or soil type or combinations of the mentioned basin characteristics. However, the distribution of each sub-catchment into different elevation and land categories is not spatially fixed. It implies that geographical information is taken from actual physical data, and is represented in each sub-catchment only as a percentage of the whole area for that sub-catchment, without keeping track of exactly where that percentage is located in space.

In the modified model version, the necessary modifications were undertaken to account for detailed basin characteristics and highly resolved meteorological variables in accordance with the objectives of the study. The HBV-IWS rainfall–runoff model was configured into a raster (grid based) form. Also, in the modified model structure the sub-catchment may be divided into a number of regular grids. The advantage of representing the sub-catchment in raster form lies in the ability to utilize high spatially resolved rainfall data and to obtain the detailed configuration of the catchment. It should be noted that the main difference between the original HBV model and the modified version is the use of regular grid cells as primary hydrological unit. Due to the modification in the model structure, snow melt, soil moisture and evapotranspiration routines are calculated for each grid cell individually. The runoff concentration processes, which are represented conceptually by reservoirs, were kept unchanged at the sub-catchment scale in order to restrict the number of model parameters to be optimized.

Data requirement

The basic input elements for the model are precipitation and air temperature. Different GIS based digital data for the catchment were obtained and appropriate processing techniques (resampling, reclassifying, and conversion of vector map into raster map) were applied in order to establish the distribution of important catchment characteristics within the study area. These data include the Digital Elevation Model (DEM) (30 m × 30 m horizontal spatial resolution), land use/land cover map (LANDSAT93 satellite images), soil map (1:200 000 scale) and river network (vector map, 1:50 000), which were obtained from the State Institute for Environmental Protection (LfU, Baden-Württemberg).

Daily precipitation and daily mean air temperature covering the study area were obtained from the German Weather Service while the daily mean discharge data for the available gauging stations was also obtained from LfU, Baden-Württemberg.

The data obtained from the meteorological stations were basically point data, and there was a need to interpolate them in order to calculate areal values for each grid. The external drift kriging method (Ahmed & de Marsily, 1987) was chosen for interpolation so that the orographic effect is taken in to account by using the topography as an additional variable. This method was utilized to generate spatially distributed precipitation and temperature data at 1 × 1 km grid resolution. Because the temperatures show a fairly constant lapse rate, topographic elevation was used as the drift variable for interpolating the temperature. It should be noted that the rate at which precipitation decreases changes with increase in elevation. The square root of the topographic elevation was assumed as a good approximation to account for such variation and it was used as the drift variable for precipitation. The collected DEM, soil map and land use map were aggregated at 1 × 1 km spatial resolution. This resolution is also the one adopted as the model grid resolution.

MATERIALS AND METHODS

The study catchment was divided into thirteen sub-catchments according to the available gauging stations. The area of the sub-catchments ranges from 120 km^2 to 614 km^2 (Fig. 1). Then the modified HBV-IWS model was set up for the study catchment based on the identified sub-catchment scheme. The interpolated precipitation was averaged over different spatial scales (2 × 2 km, 3 × 3 km, 4 × 4 km and 5 × 5 km) and at the sub-catchment scales. Two different simulation experiments were conducted to predict the uncertainty due to spatial variability of precipitation. In the first experiment the model was calibrated on 1 × 1 km model resolution with all the forcing variables at the same model resolution and run using the averaged precipitation over different spatial resolutions. In the second simulation experiment, the model was calibrated with the uniform precipitation obtained from each sub-catchment. Hence, the model grids located within each sub-catchment were assigned the same uniform averaged precipitation obtained for the individual sub-catchment. Thereafter, the calibrated model was run using the interpolated precipitation at 1 × 1 km spatial resolution and the averaged precipitation over different spatial scales ranging from 4 km^2 to 25 km^2. In this simulation experiment the model resolution was also attained at 1 × 1 km.

Finally, a set of simulations was carried out using the conditionally simulated precipitation. The conditional simulated precipitation (Cressie, 1993) was produced by the means of turning band simulation was utilized in the calibrated model using the 1 × 1 km grid precipitation at 1 × 1 km model resolution.

Calibration of the model

The automatic calibration of the distributed version of the HBV-IWS model was accomplished based on the concept of hydrological response unit (geoclass). The geoclasses were defined on the basis of soil and land use information. The collected soil map (SC) and land use map (LC) was reclassified into a smaller number of classes. The above-mentioned basin characteristics were combined in 28 geoclasses (7 SC × 4 LC). The parameters used in the soil module include the field capacity, permanent wilting point and beta (conceptual model parameter). These parameters were optimized based on the geoclasses. Also, the parameter values were predefined within a feasible parameter interval, which was adjusted to allow different degrees of freedom. In addition, optimized parameters corresponding to the 28 geoclasses were assigned to the grids. It should be noted that grids under similar geoclasses would have the opportunity to receive the same value. During calibration, other parameters like degree day factor and threshold temperature (in the snow module) were optimized and kept constant through the study area while the reservoir parameters were optimized for individual sub-catchments.

RESULTS AND DISCUSSION

The distributed HBV-IWS model was automatically calibrated (calibration period: 1 January 1961 to 31 December 1970) by means of the combinatorial optimization algorithm simulated algorithm annealing (Aarts & Korst, 1989). For maximization at different temporal scales (daily scale, daily scale weighted to the maximum discharge and annual scale), the objective function used was the aggregated Nash-Sutcliffe coefficients.

Also, the simulation results were compared using the Nash-Sutcliffe coefficient (R^2) (Nash & Sutcliffe, 1970) given as:

$$R^2 = 1 - \left(\frac{(q_s(t) - q_o(t))^2}{(q_o(t) - q_m)^2} \right) \tag{1}$$

where $q_o(t)$ is the observed daily discharge ($m^3\ s^{-1}$), $q_s(t)$ is the simulated daily discharge ($m^3\ s^{-1}$) and q_m is the mean observed daily discharge ($m^3\ s^{-1}$).

The Pearson correlation coefficient (*Corr.*) was computed to measure the strength of the linear relationship between simulated and observed discharge time series.

$$Corr. = \frac{(q_s - \overline{q}_s)(q_o - \overline{q}_o)}{\sigma_s \sigma_o} \tag{2}$$

where σ_s and σ_o are the standard deviations of simulated and observed discharge,

respectively. $\overline{q_s}$ and $\overline{q_o}$ are the mean of simulated and observed daily discharge, respectively.

The relative accumulated difference and the peak error were also computed to judge the performance of the model with regard to maintaining the water balance and its peak flow estimation capacity. Accordingly the relative accumulated difference (*RD*) is computed as:

$$RD = \frac{\sum q_s - \sum q_o}{\sum q_o} \tag{3}$$

and the peak error is equal to:

$$peakError = \frac{\overline{q}_{s(\max)} - \overline{q}_{o(\max)}}{\overline{q}_{o(\max)}} \tag{4}$$

where $\overline{q}_{s(\max)}$ is the mean annual maximum simulated discharge and $\overline{q}_{o(\max)}$ is the mean annual maximum observed discharge.

The mentioned goodness-of-fit indexes were computed on an annual and seasonal basis for the overall validation period (1 January 1971 to 31 December 1980).

The calibrated model, using the 1 × 1 km grid precipitation was utilized with averaged precipitation for the validation period. Table 1 summarizes the model performance at two selected sub-catchments namely Horb and Plochingen (outlet gauge). Also, it is noticed that no significant differences were observed in the calibrated model performance using 1 × 1 km grid precipitation and averaged precipitation at different spatial scales. This may be due to the fact that the averaged precipitation was obtained from the interpolated precipitation (external drift kriging) which is already a smoothed rain field. Figure 2 shows the model performance at Horb in different seasons for the validation period. Meanwhile, the model performance was comparatively poor in the summer season due to the convective precipitation, which was not well captured by the existing coarse raingauge networks.

The distributed HBV-IWS model was calibrated in this simulation experiment using averaged precipitation from each of the sub-catchments. The model resolution during this calibration was also 1 × 1 km. The calibrated model was utilized with the precipitation averaged at different spatial scales for the validation period. Table 2

Table 1 Model performance with different resolutions of precipitation utilized to calibrated model using the 1 × 1 km grid precipitation.

Resolution of precipitation (km^2)	Catchment #3: Horb				Catchment #13: Plochingen			
	R^2	Corr.	*RD*	Peak error	R^2	Corr.	*RD*	Peak error
4	0.752	0.874	0.121	–0.113	0.796	0.896	0.087	–0.099
9	0.752	0.875	0.121	–0.113	0.796	0.896	0.087	–0.099
16	0.752	0.874	0.122	–0.113	0.796	0.896	0.087	–0.100
25	0.752	0.874	0.123	–0.120	0.796	0.894	0.088	–0.101
420.18 [#3] 472.05 [#13]	0.751	0.870	0.124	–0.125	0.792	0.897	0.087	–0.114
1	0.753	0.874	0.116	–0.112	0.798	0.899	0.081	–0.099

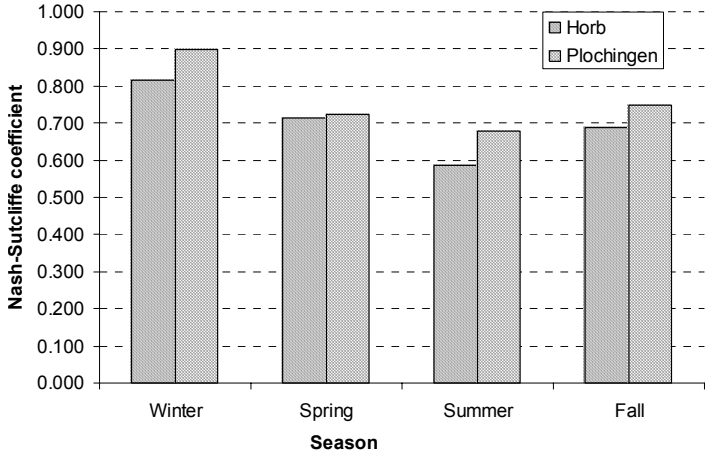

Fig. 2 Model performance at Horb in different seasons for the validation period.

Table 2 Model performance with different resolutions of precipitation utilized to calibrated model using the sub-catchment averaged precipitation.

Resolution of precipitation (km^2)	Catchment #3: Horb				Catchment #13: Plochingen			
	R^2	Corr.	*RD*	Peak error	R^2	Corr.	*RD*	Peak error
1	0.748	0.874	0.127	–0.118	0.791	0.893	0.089	–0.104
4	0.751	0.873	0.124	–0.143	0.790	0.894	0.111	–0.106
9	0.751	0.873	0.126	–0.145	0.790	0.893	0.124	–0.119
16	0.750	0.873	0.131	–0.133	0.790	0.890	0.119	–0.115
25	0.750	0.869	0.130	–0.142	0.784	0.886	0.115	–0.121
420.18 [#3] 472.05 [#13]	0.746	0.873	0.142	–0.150	0.763	0.894	0.114	–0.168

summarizes the model performance in relation to the present simulation experiment. Comparing the results of the two experiments, it can be noticed that the model performance deteriorated while the model was calibrated with sub-catchment averaged precipitation instead of 1 × 1 km grid precipitation.

The conditional simulated precipitation (Cressie, 1993) by means of turning band simulation, was utilized for the calibrated model using the 1 × 1 km grid precipitation at 1 × 1 km model resolution. A detailed representation of the performance of the HBV-IWS model with correspondence to the maximum, minimum and mean of several realizations of simulated precipitation is given in Fig. 3 for selected flood peaks in the validation period at the Horb gauge. The hydrograph resulting from the maximum of the realizations of the simulations was worse when considering the entire period; however it was better if only the floods were considered, as Fig. 3 shows.

CONCLUSIONS AND FUTURE WORK

A new raster (grid) based version of the HBV-IWS model was developed in order to assess the influence of the spatially distributed precipitation variability on the accuracy of simulated runoff.

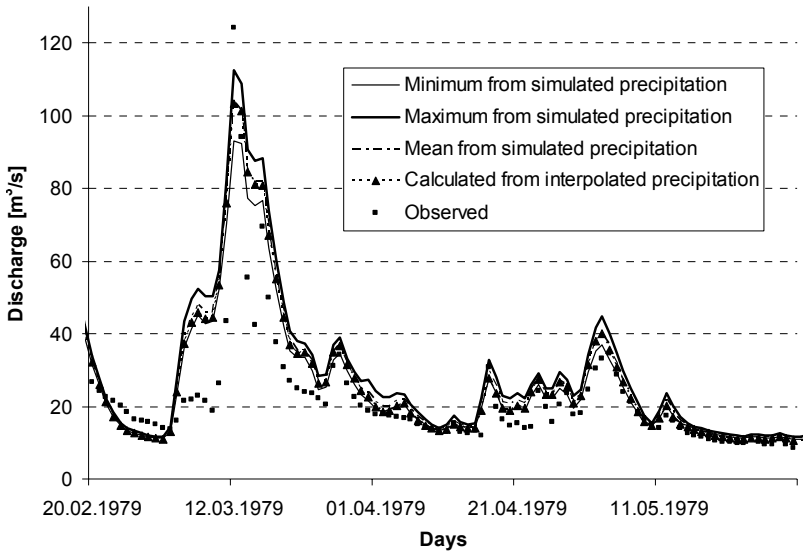

Fig. 3 Comparisons between calculated discharges from interpolated precipitation and conditionally simulated precipitation with observed discharge at Horb in the validation period.

The application to the Upper Neckar catchment showed that there is no significant difference in the calibrated model performance using 1 × 1 km grid precipitation and averaged precipitation on different spatial scales. This may be due to the fact that the averaged precipitation was obtained from the interpolated precipitation (external drift kriging) which is already a smoothed rain field and existence of the coarse raingauge network. In contrast, minimal model performance improvements were observed when the calibrated model was utilized with comparatively detailed precipitation data. The model performance slightly deteriorated when the model was calibrated with sub-catchment averaged precipitation instead of 1 × 1 km grid precipitation.

Conditional simulation assures a more accurate representation of rainfall variability as compared to interpolated rain fields due to smoothing effects. Peak estimations derived using simulated precipitation are superior to the same obtained using interpolated precipitation. Spatial simulation is thus reasonable for flood forecasting.

Future research will be performed to obtain a better perspective of the precipitation integration on the predictive uncertainty of a rainfall–runoff model using radar rainfall data in addition to raingauge data.

REFERENCES

Addeland, I., Matheussen, B. V. & Lettenmaier, D. P. (2002) Influence of spatial resolution on simulated streamflow in a macroscale hydrologic model. *Water Resour. Res.* **38**(7), 29.1–29.10.

Ahmed, S. & de Marsily, G. (1987) Comparison of geostatistical methods for estimating transmissivity using data on transmissivity and specific capacity. *Water Resour. Res.* **23**(9), 1717–1737.

Aarts, E. & Korst, J. (1989) *Simulated Annealing and Boltzmann Machines A Stochastic Approach to Combinatorial Optimization and Neural Computing*. John Wiley & Sons, Chichester, UK.

Bergström S. & Forsman A. (1973) Development of a conceptual deterministic rainfall–runoff model. *Nordic Hydrol.* **4**, 174–170.

Cressie, Noel A. C. (1993) *Statistics for Spatial Data*. John Wiley & Sons, New York, USA.

Finnerty, B. D., Smith, M. B., Seo, D .J., Koren, V. & Moglen, G. E. (1997) Space-time scale sensitivity of the Sacramento model to radar-gage precipitation inputs. *J. Hydrol.* **203**, 21–38.

Krajewski, W. F., Lakshmi, V., Georgakakos, K. P. & Jain, S. C. (1991) A Monte Carlo study of rainfall sampling effect on a distributed catchment model. *Water Resour. Res.* **27**(1), 119–128.

Liang, X., Guo, J. & Leung L.R. (2004) Assessment of the effects of spatial resolutions on daily water flux simulations. *J. Hydrol*. **298**, 287–310.

Lopes, V. L. (1996) On the effect of uncertainty in spatial distribution of rainfall on catchment modelling. *Catena* **28**, 107–119.

Nash, J. E. & Sutcliffe, J. V. (1970) River flow forecasting through conceptual models. Part I. A discussion of principles. *J. Hydrol.* **10**, 282–290.

Obled, C. H., Wendling, J. & Beven, K. (1994) The sensitivity of hydrological models to spatial rainfall patterns: an evaluation using observed data. *J. Hydrol*. **159**, 305–333.

Smith, J. A., Seo, D. J., Baeck, M. L. & Hudlow, M. D. (1996) An intercomparision study of NEXRAD precipitation estimates. *Water Resour. Res*. **32**(7), 2035–2045.

Wilson, C. B., Valdes, J. B. & Rodriguez-Iturbe, I. (1979) On the influence of the spatial distribution of rainfall on storm runoff. *Water Resour. Res.* **15**(2), 321–328.